ORIGINAL PAPER

International Journal of Occupational Medicine and Environmental Health 2023;36(2)
https://doi.org/10.13075/ijomeh.1896.01913

NUMERICAL AND CLINICAL ANALYSIS OF AN EYEBALL INJURIES UNDER DIRECT IMPACT

MATEUSZ KOBERDA[1], ANDRZEJ SKOREK[2], PAWEŁ KŁOSOWSKI[3], MARCIN ŻMUDA-TRZEBIATOWSKI[3], KRZYSZTOF ŻERDZICKI[3], PAWEŁ LEMSKI[2], and URSZULA STODOLSKA-KOBERDA[1]

[1] Medical University of Gdańsk, Gdańsk, Poland
Department of Ophthalmology
[2] Medical University of Gdańsk, Gdańsk, Poland
Department of Otolaryngology
[3] Gdańsk University of Technology, Gdańsk, Poland
Department of Mechanics of Materials and Structures, Faculty of Civil and Environmental Engineering

Abstract
Objectives: The objective of this study was to develop a numerical model of the eyeball and orbit to simulate a blunt injury to the eyeball leading to its rupture, as well as to conduct a comparative analysis of the results obtained using the finite element method against the clinical material concerning patients who had suffered an eyeball rupture due to a blunt force trauma. **Material and Methods:** Using available sclera biometric and strength data, a numerical model of the eyeball, the orbital contents, and the bony walls were developed from the ground up. Then, 8 different blunt force injury scenarios were simulated. The results of numerical analyses made it possible to identify possible locations and configurations of scleral rupture. The obtained results were compared against the clinical picture of patients hospitalized at the Department of Ophtalmology, Medical University of Gdańsk in 2010–2016 due to isolated blunt force trauma to the eyeball. **Results:** It has been demonstrated that the extent of damage observed on the numerical model that indicated a possible location of eyeball rupture did not differ from the clinically observed configurations of the scleral injuries. It has been found that the direction of the impact applied determines the location of eyeball rupture. Most often the rupture occurs at the point opposite to the clock-hour/positions of the impact application. The eyeball rupture occurs in the first 7–8 ms after the contact with the striking rigid object. It has been established that the injuries most often affected the upper sectors of the eyeball. Men are definitely more likely to sustain such injuries. Eyeball ruptures lead to significant impairment of visual acuity. **Conclusions:** This study may contribute to a better understanding of injury mechanisms and better treatment planning. It may also contribute to the development of eyeball protection methods for employees exposed to ocular injuries. Int J Occup Med Environ Health. 2023;36(2)

Key words:
trauma, numerical model, finite element method, blunt force trauma, eyeball rupture, eye protection

INTRODUCTION

Each case of vision impairment resulting from injury has serious consequences both in terms of the quality of life of the injured person and from the occupational and socioeconomic point of view. According to the World Health Organization (WHO), around 55 million eye injuries occur worldwide each year, of which about 1.6 million (about 3%) cases result in blindness [1]. According

Funding: this research was supported by Grant OPUS 12 No. 2016/23/B/ST8/00115 "Analysis of the mechanical properties of the eye orbital wall and the numerical nonlinear dynamic analysis of the orbital blow-out trauma type verified by clinical observations," provided by National Science Centre (NCN), Kraków, Poland.
Received: September 5, 2021. Accepted: March 20, 2023.
Corresponding author: Andrzej Skorek, Medical University of Gdańsk, Department of Otolaryngology, Smoluchowskiego 17, 80-952 Gdańsk, Poland (e-mail: andrzej.skorek@gumed.edu.pl).

to these statistics, the largest percentage of injuries is blunt force trauma, followed by injuries from a sharp object, traffic accidents, gun shooting, injuries involving pyrotechnics, and falls [2,3]. According to US statistics nowadays accidents take place mostly at home (41%), accidents at workplace are the second most common (14%) [2]. For less developed countries this statistics is different and work-related injuries are more common. The worst prognosis is for injuries resulting from assault/beating and injuries sustained in motorcycle accidents [4]. Additionally, it has been demonstrated that the state under the influence of alcohol is not only conducive to the occurrence of serious eye injury but also tends to worsen the prognosis when the injury occurs [5].

Work-related eye injuries can be categorized as traumatic injuries and exposure injuries. The former are for example blunt or penetrating trauma to the eyeball and/or surrounding structures such as orbit and/or lids – corneal abrasions and foreign bodies, scleral abrasions, lacerations to the lids and lid margins, damage to the tear duct apparatus and globe laceration. Penetrating injuries may result in an intraocular foreign body. Blunt eye injury during work duties mainly occur when tools slip malfunction and strike the globe. Direct blunt trauma to the globe may result in the formation of a hyphema, development of retrobulbar hemorrhage and orbital compartment syndrome or in most serious cases may lead to globe rupture. The latter include for example thermal burns, electric arc injuries, ultraviolet light exposure, laser light burns and acid or alkali burns (alkali burns and tend to be more serious than acid burns because they penetrate soft tissues deeper).

In the literature, the number of eyeball injuries in men is much higher than in women. The most frequently reported amount is 4 times the amount [2,3]. This statistic fully corresponds to the number of eyeball fractures in the clinical material analyzed for this study, which showed an identical ratio of trauma in men and women. However, if all injuries are analyzed and not limited to eyeball rupture, the percentage of women is more modest and amounts to 12.2%. This number is also very similar to the report by Stafiej et al. [6] from the Department of Ophthalmology in Bydgoszcz, Poland, 2001–2003. This can be explained by a different gender distribution of causes for hospitalization. Namely, men are much more often hospitalized due to the penetration of foreign bodies into the eye tissue and orbit or perforating or penetrating injuries, which is related to the nature of their work (miner, locksmith, mechanic, etc.) performed predominantly by men. Women, on the other hand, suffer more blunt injuries than with a sharp object. The above work also mentions that half of the injuries occur at home, one third at work and the rest elsewhere. In the case of the material of the Ophthalmology Department of University Clinical Center in Gdańsk, Poland, the statistics regarding eyeball fractures indicate that only 8.3% occurred during work. However, if all cases of injuries are taken into account, indeed approx. 36% (109 patients) took place while performing work, while more than half (56.8%) took place at home or in its immediate vicinity.

Injuries in children are a separate clinical problem. Among them, a particularly important mechanism that disrupts the scleral continuity is a penetrating trauma with a sharp object as well as blunt force injuries. The most common cases included accidental mutilation, violence, and transport-related injuries [7]. Many of such injuries could have been avoided with proper eye protection.

Smith and Regan proposed 2 theories to describe the pathomechanism of orbital injury in the course of impact with a blunt object, i.e., the buckling theory and the hydraulic theory [8]. The buckling theory assumes an orbital wall fracture when the force is applied to the outer rim. On the other hand, the hydraulic theory explains the formation of fractures of the lower and/or medial orbital wall, while the orbital wall remains intact.

According to this theory, forces acting on the orbital soft tissues move them backwards, leading to the creation of pressure which is transferred evenly to all orbital walls, and their rupture usually occurs in the thinnest place [9,10]. The study by Ahmad et al. proves that such an injury mechanism protects the eyeball from rupture as a result of blunt trauma [11]. In that study, it was found that less force was needed to break the orbital floor when the force was applied directly to the eyeball than when it was applied to the orbital rim. The orbital contents together with the eyeball and bony walls are closely interrelated in terms of mechanics. Most of the studies on eyeball resistance to injuries concerned models of the eyeball alone [12–15]. Accurate mapping of the orbital contents influences the value of results of modeling dynamic blunt trauma both to the eyeball and the orbit, as well as the conclusions drawn from such experiments [16].

Objective of the study

Studies on the mechanisms of blunt trauma, its course, and its effect bring us closer to the invention of more effective methods of eye protection at work, more accurate diagnostics and possibly better treatment methods. For obvious reasons, such studies cannot take place *in vivo*, which is why they are increasingly often conducted on numerical models. This study aimed to present some aspects of numerical modeling of the eyeball and orbit and the elements of analysis of simulated blunt injury caused by a moving, rigid object (cylindrical shape). The results obtained with simulation methods were compared against clinical studies of patients with eyeball rupture hospitalized at the Department of Ophthalmology at the University Medical Center of Gdańsk.

MATERIAL AND METHODS

For the needs of the analysis, the properties of individual parts of the orbit and eyeball (except for the sclera) were adopted as per literature (Table 1). For the sclera, the elastic modulus (Young's modulus) value of 10.7 MPa was adopted, being the average from the previously conducted own tests (on an animal specimens) [16]. Then, the orbital numerical model was constructed. The possibility of contact between the following elements was determined: the rigid cylinder and the outside of the eyeball, the eyeball and the orbital fat, and the fat and the bone. Also, a membrane representing the orbital septum was created. From a mechanical point of view, it was assumed that both the eyeball interior the orbital fat were incompressible materials, which reflects the Poisson modulus value close to 0.5, and that bones, eyeball, and adipose tissue were elastic isotropic materials. Adoption of the Poisson modulus value $\nu = 0.49$ for incompressible elements caused a divergence of calculations. Only the value of $\nu = 0.499999$ led to correct results [17,18].

To obtain the most reliable and life-like results, in the finite element analysis a geometrically nonlinear variant in the range of large deformations was used in

Table 1. Material properties adopted for the individual elements of the eyeball and orbit model based on the literature

Element	Reference	Young's modulus [Pa]	Poisson modulus (ν)	Density [kg/m^3]
Orbital bones	10	1.3×10^9	0.33	2000
Vitreous body	20, 28	0.5×10^6	0.499999	1000
Orbital fat	16	0.5×10^6	0.499999	952
Sclera and cornea	16, 28	10×10^6	0.42	1000
Orbital septum	16	0.5×10^6	0.33	1000

the Lagrange approach. In the MSC Marc/Mentat program (MSC Software, Newport Beach, California, USA), dynamic calculations were performed in the dynamic implicit options. The equations of motion were integrated using the Houbolt method with the parameters $\gamma_1 = 1.5$ and $\gamma = -0.5$. The integration step was $\Delta t = 10^{-6}$ s. Moreover, it was assumed that all materials are isotropic and have elastic (bones) or elastic perfect plastic (soft tissues) physical properties (Table 1). Nevertheless, the analysis was terminated when the elastic limit of the sclera was reached at a certain point. It was assumed that it is the eyeball rupture point.

The obtained results were displacements, stress components, and equivalent stresses Huber-von Mises-Hencky σ_M calculated according to the formula:

$$\sigma=\frac{1}{\sqrt{2}}\sqrt{(\sigma_x-\sigma_y)^2+(\sigma_y-\sigma_z)^2+(\sigma_z-\sigma_x)^2+6(\tau_{xy}^2+\tau_{xz}^2+\tau_{yz}^2)}\leq R_{KT} \quad (1)$$

where:

σ_x, σ_y, σ_z – normal stress consistent with the axes of the global coordinate system;

τ_{xy}, τ_{xz}, τ_{yz} – shear stress in the same system;

R_{KT} – ultimate stress value causing sclera rupture.

The application of this hypothesis is because only one parameter is known, determining the moment of sclera rupture. In the obtained analyses, no stress component exceeded the permissible value of R_{KT}, but the already calculated equivalent stresses σ_M exceeded these permissible values, and it was possible to end the simulation at this stage and recognize that the sclera ruptured.

The sclera and cornea were modeled as separate parts of the eyeball since they feature different mechanical properties. For simplicity, eye lens was not included in the modeling due to their complicated suspension system and a minor role it could play in eyeball rupture.

The phenomenon of contact was taken into account in the calculations. For this purpose, 4 deformable bodies were defined: bone, eyeball, orbital septum and fat, and a single rigid body (or "punch") that caused the system deformation. To build the model (Figure 1), the authors adopted equations for curvatures of individual eyeball structures included in the work [19].

First to check numerical properties of the eyeball model, which was the most important part of analysis, it was tested alone using a non-linear dynamic compression test on a rigid surface (Figure 2).

Our model consists of 22 673 nodes and 98 064 elements (of which 32 346 for the eyeball). The finished model of the eyeball was linked to the other elements of the orbit and a rigid cylinder. This object was to strike at the eye-

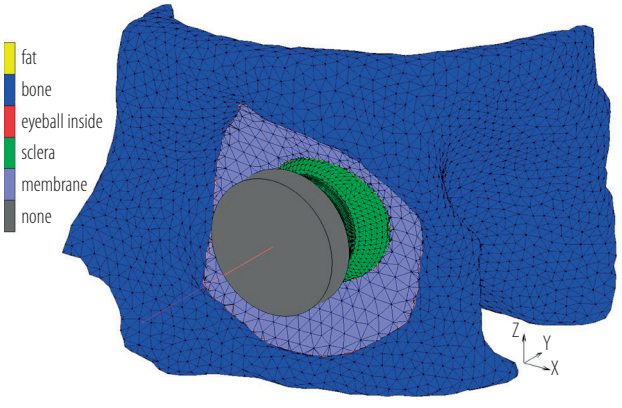

Figure 1. Finished model of the eyeball, orbit and striking object

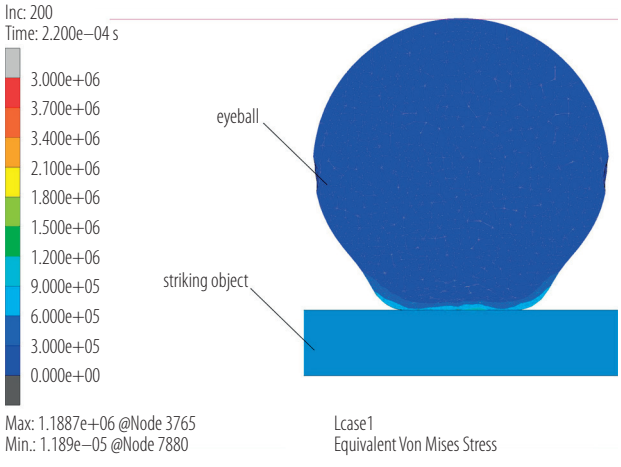

Figure 2. Test of the eyeball numerical model [Pa]

Table 2. Initial velocity vectors for the individual tests

Test[a]	Velocity vector [m/s]		
	component X	component Y	component Z
0°–0°	0	9	0
45°–0°	–6.364	6.364	0
30°–0°	–4.57	7.7942	0
15°–0°	–2.3294	8.6933	0
0°–5°	0	8.69333	2.32937
30°–15°	–4.34667	7.52865	2.32937
15°–15°	–2.25	8.39711	2.32937

Component X, Y, Z according to the global coordinate system (Figure 1).
[a] [y axis dev.] – [z axis dev.] / axis.

ball directly at a speed of 9 m/s and then decelerate linearly to 0 m/s after 0.003 s. Eight tests were performed from 8 different directions. The finite element mesh is shown in (Figure 1). Velocity vectors for the specified impact directions are presented in Table 2.

RESULTS

Finite element modeling of the eyeball rupture

The solution for finite element equations was obtained in the form of stress maps in the numerical model of the eyeball. It should be noted that all of the tests were performed for the left eyeball and left orbit model. In each test, the rigid cylinder stroke at the eyeball from a different direction. The numerical model indicated the points, where the assumed stress limit was achieved, identical to the most likely point of scleral rupture *in vivo* (Table 3). Following other authors' reports, for the limit stresses resulting in scleral rupture the following values were adopted: strain $\varepsilon = 6.8\%$; stress $R_K = 9.4$ MPa [13,20].

Comparison with clinical data

The locations of eyeball rupture in patients hospitalized in the Ophthalmology Department of University Medical Center of Gdańsk in 2010–2016 were determined, as illustrated in Table 4.

Table 3. Summary of tests on the numerical model

Test	Impact direction	Limit stress reaching reference point	Limit stress reaching time [h]
Test 1 (0°–0°)	from the front (along axis Y)	sclera in the place of the external rectus muscle attachment	3:00
Test 2 (45°–0°)	from the front at an angle of 45° from axis Y (from the front and the temple)	sclera in the nasal quadrant in the projection of the flat part of the ciliary body (pars plana), slightly below the height of the internal rectus muscle attachment	8:30
Test 3 (30°–0°)	from the front at an angle of 30° from axis Y (from the front and the temple)	sclera in the nasal quadrant in the projection of the flat part of the ciliary body (pars plana), slightly below the height of the internal rectus muscle attachment	8:30
Test 4 (15°–0°)	from the front at an angle of 15° from axis Y (from the front and the temple)	sclera in the nasal quadrant in the projection of the flat part of the ciliary body (pars plana), slightly below the height of the internal rectus muscle attachment	8:30
Test 5 (0°–15°)	from the front along axis Y and from below at an angle of 15° from axis Z (from below)	sclera in the upper quadrant, in the pars plana projection, in the projection of the upper rectus muscle attachment	11:00–12:00
Test 6 (30°–15°)	from the front at an angle of 30° from axis Y and from below at an angle of 15° from axis Z (from the temple and from below)	sclera in the upper quadrant, in the pars plana projection, slightly nasally from the upper rectus muscle attachment	11:00–12:00
Test 7 (15°–15°)	from the front at an angle of 15° from axis Y and from below at an angle of 15° from axis Z (from the temple and from below)	sclera in the upper quadrant, the pars plana projection, in 2 places: slightly nasally and slightly temporally from the projection of the upper rectus muscle attachment	11:00, 01:00

Table 4. Summary of clinical cases

Participant (No.)	Sex	Age [years]	Eyeball	Mechanism of trauma	Rupture location	Rupture extent
1	M	67	left	impact (wood fragment)	corneal limbus	6:00–10:00
2	M	78	left	fall (on the pot) impact (beating)	muscle attachment + to the equator	9:00–12:00
3	M	41	left	impact (beating)	corneal limbus	4:00
4	M	59	right	impact (beating)	muscle attachment	12:00–3:00
5	M	62	left	fall (onto heater)	corneal limbus	10:00–12:00
6	M	61	right	impact (wood trunk)	corneal limbus + meridian wound	11:00–6:00
7	M	67	right	strike (sole)	corneal limbus + oblique wound	10:00–2:00
8	F	70	right	fall (on bathroom faucet)	corneal limbus	11:00–4:00
9	M	58	right	fall (getting off the bus)	equator	9:00–12:00 (90° in the upper temporal quadrant)
10	M	64	left	bash (metal object)	corneal limbus + 2 meridian wounds	1:00–4:00 + meridional wounds at 1:00 and 4:00 almost to n. II
11	M	60	right	impact (beating)	equator towards the back of the eyeball	12:00–3:00 obliquely towards the rear pole
12	M	54	left	impact (beating)	corneal limbus	10:00–2:30
13	M	65	right	fall	corneal limbus	6:00–12:00
14	M	26	right	impact (hit by the car)	pars plana	1:00–2:30
15	F	69	right	impact (with wood)	corneal limbus	1:00–6:00
16	F	53	left	impact (chair rod)	corneal limbus + meridian	6:00–12:00 and then to the upper rectus muscle
17	M	60	left	fall (edge of well)	corneal limbus	12:00–5:00
18	M	60	right	impact (probably against the steering wheel)	equator	9:00–1:00
19	M	41	right	impact (with a piece of wood)	meridian from the limbus to the equator	7:00
20	M	59	right	bang (champagne cork)	corneal limbus	9:00
21	F	60	right	fall	corneal limbus + meridian wound	7:00–12:00
22	M	54	right	impact (beating)	equator	9:30–12:00
23	M	10	right	impact (shovel)	corneal limbus + oblique wound	7:30–12:00
24	M	64	left	impact (against the corner of the shelf)	upper rectus muscle attachment	12:00

The data obtained in the analysis of the clinical material (Table 4) were compared against the data obtained in the dynamic analysis on the numerical model (Table 3), and such configurations of eyeball rupture in clinical patients were selected that correspond to the results of the numerical simulation regarding the location of

Table 5. Comparison of the tests on the numerical model with the clinical cases

Test	Limit stress reaching time [h]	Patient with a similar rupture (No.)
Test 1 (0°–0°)	3:00	3, 20
Tests 2 (45°–0°), 3 (30°–0°), 4 (15°–0°)	8:30	1
Test 5 (0°–15°)	11:00–12:00	11, 24
Test 6 (30°–15°)	11:00–12:00	2, 4, 5, 8, 14
Test 7 (15°–15°)	11:00, 1:00	7, 12

the probable rupture, as presented in Table 5. The selected ones were presented in the form of legible figures (Figure 3–8).

In half of the patients (No. 3, 6, 9, 10, 13, 15–19, and 21–23 as per Table 4), no rupture configuration matching the locations indicated in the numerical simulation was observed, or the rupture size was too large to indicate the probable original rupture spot. Most likely, a mechanism of injury in these patients was complex, or the impact directions varied from those proposed in Table 3.

All procedures related to this research work have been positively assessed by the Independent Bioethical Committee for Scientific Research at the Medical University of Gdańsk (NKBBN/497/2016).

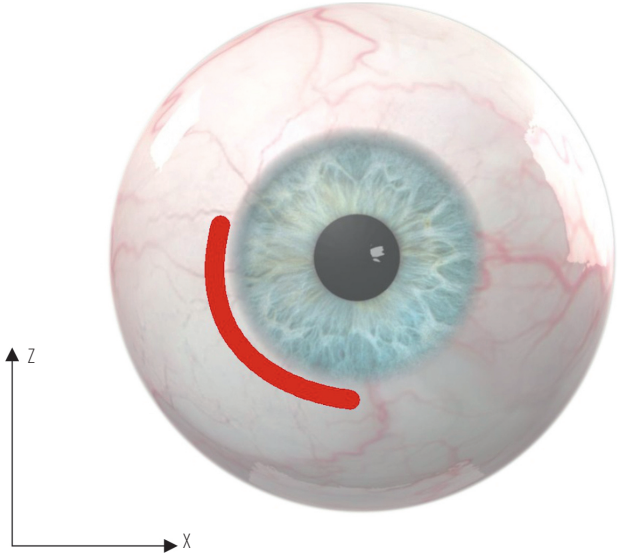

Figure 4. Location of the wound in patient No. 1 (left eye)

DISCUSSION

The literature describes various objectives and applications for eyeball numerical models. Nagasao et al. [21], Schaller et al. [22], and Al-Shukhun et al. [23] were the first ones to use mathematical methods (finite element method) for orbital model construction. Initially, the models contained only bony elements. Later on, they were enriched with orbital contents (eyeball and other retrobulbar structures) [21–27]. More advanced models were built based on the CT image transferred

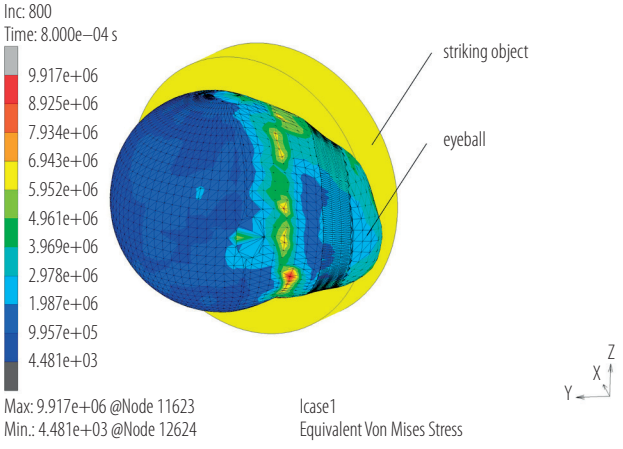

Figure 3. Predicted sclera rupture site in test No. 2 [Pa]

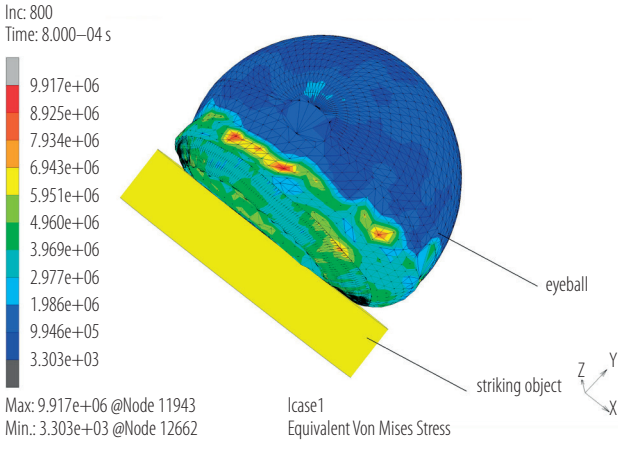

Figure 5. Predicted sclera rupture site in test No. 5 [Pa]

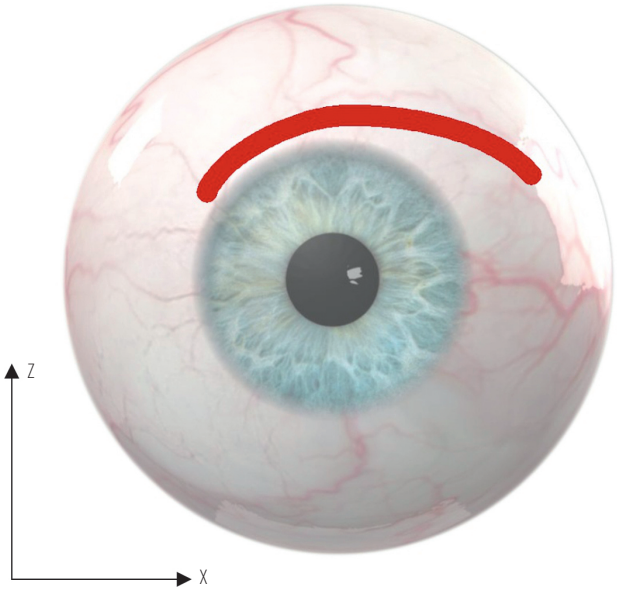

Figure 6. Location of the wound in patient No. 7 (right eye)

with the use of computational programs to a mathematical finite element model. The basis for the data transfer were grayscale (Hounsfield scale) units, considering only the linear coefficient for the weakening of density and not the material properties of the tissues. Those studies made it possible to obtain a new perspective on the traumatology of the orbit. For this reason, it was possible to assess the behavior of individual bone structures in the course of injury and find *locus minoris resistentie* of the orbit, as well as to determine particularly dangerous injury directions. From here, it is only a step to develop new protective measures for people who are particularly exposed to damage to the orbit, both in the workplace and during sports activities. However, the modeled orbital contents were treated as a kind of "filling" for bone structures, without high accuracy in the mapping of the eyeball, for example.

In the work by Gray et al. [15], the objective was to compare the results of numerical modeling of an eye injury from a paintball impact with the empirical model of such an injury. In that work, an exact model of the eyeball was built, and consistency of the numerical model

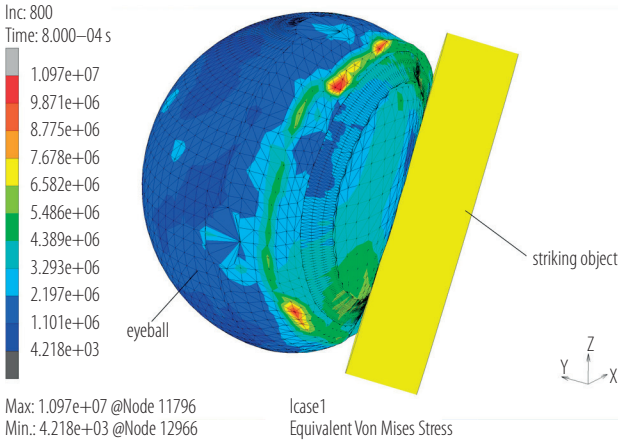

Figure 7. Predicted sclera rupture site in test No. 6 [Pa]

with the trauma course observed using high-speed cameras was demonstrated. Since ballistic tests require placing an examined eyeball in a block of transparent gel, the numerical model of the eye in that study was placed in similar conditions. Also, the authors demonstrated that numerical modeling of trauma could help in the understanding of the course and causes of intraocular injuries that have not yet been precisely explained. In the work by Dai et al. [28], the numerical model was used to further explain the mechanisms of drug transport from the eye

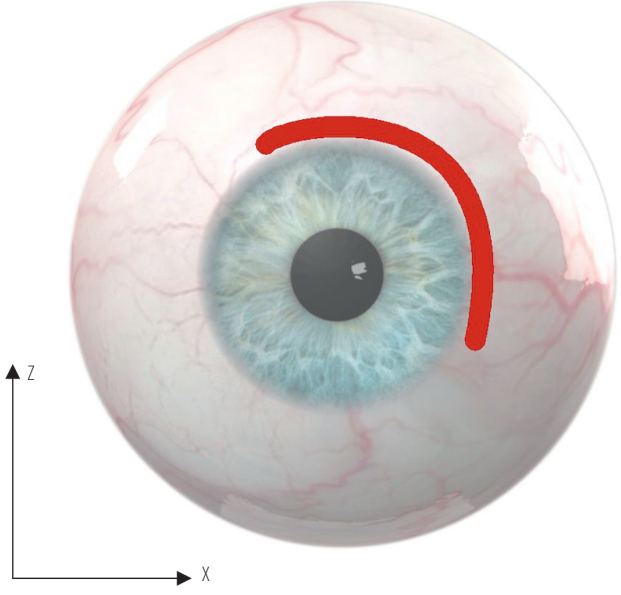

Figure 8. Location of the wound in patient No. 8 (right eye)

surface to the anterior chamber, and the purpose of those studies was to contribute to improving the effectiveness of drugs administered in that way.

The innovation of our study lies in the fact that in none of the so-far published works the numerical model of the eyeball embedded in a numerical model of the orbit of a real patient was compared against clinical cases.

Studies on the mechanisms of blunt trauma, its course and its effects certainly bring us closer to determining more effective methods of eye protection especially in work environment. For obvious reasons, such studies cannot take place *in vivo*, which is why they are increasingly often conducted using numerical models. In our work, some aspects were presented concerning numerical modeling of the eyeball and orbit as well as elements of the analysis of simulated blunt trauma caused by a moving rigid object. The results obtained with simulation methods were compared against clinical studies of patients with eyeball rupture hospitalized at the Department of Ophthalmology at the University Medical Center of Gdańsk. The largest extent of damage was observed both in the numerical model and in patients in the cases of strokes presented as test No. 7 (15°/15°). It seems that this should be taken into account in studies on the construction of eye protection elements.

CONCLUSIONS

The tests performed suggest that in the case of a blunt impact directly at the eyeball with an object moving at a speed of about 9 m/s from a specific direction, the eyeball rupture will begin at a specific and repetitive location. This knowledge can be used in situations where the configuration of the eyeball rupture is known but it is necessary to determine the direction from which the impact might have occurred.

The results of the analysis on the created numerical model can be compared against real eyeball ruptures observed in patients in hospital conditions. In many cases, the rupture configuration is consistent with the simulated rupture sites; however, this comparison cannot be applied for extensive ruptures, but only for those limited to 2–3 clock-hours distance of the sclera. This is because for more extensive wounds it is not possible, at the current stage of research, to determine the direction of rupture widening, therefore it cannot be presumed which clock-hour of the rupture was the initial, and which one was the terminal point of the rupture.

The limit stress on the created numerical model was achieved no later than after 8 ms from the contact of the object striking at the cornea of the modeled eyeball. This observation suggests that the sclera begins to rupture before the impact pulse stops acting.

Further development of the numerical model details to include periocular muscles and other so-far omitted structures (such as crystalline lens), while considering the plasticity effect or, finally, including the damage phenomenon in simulations, will result in obtaining more accurate results and lead to drawing more far-reaching conclusions.

REFERENCES

1. Négrel AD, Thylefors B. The global impact of eye injuries. Ophthalmic Epidemiol. 1998;5:143–69.
2. May DR, Kuhn FP, Morris RE, Witherspoon CD, Danis RP, Matthews GP, et al. The epidemiology of serious eye injuries from the United States Eye Injury Registry. Graefes Arch Clin Exp Ophthalmol. 2000;238:153–7.
3. MacEwen CJ, Baines PS, Desai P. Eye injuries in children: the current picture. Br J Ophthalmol. 1999;83:933–6.
4. Liggett PE, Pince KJ, Barlow W, Ragen M, Ryan SJ. Ocular trauma in an urban population. Review of 1132 cases. Ophthalmology. 1990;97:581–4.
5. Jian-Wei L, Zhen-Bo H, Shu-Na W, Yu-Guang Z, Ai-Jun D. The clinical characteristics of alcohol-related ocular rupture. Graefes Arch Clin Exp Ophthalmol. 2015;253:1307–11. https://doi.org/10.1007/s00417-014-2809-x.

6. Stafiej J, Malukiewicz-Wiśniewska G, Czajkowski G. [Open globe injuries--selected epidemiologic features in own material]. Klin Oczna. 2005;107:243–6. Polish.
7. Lesniak SP, Bauza A, Son JH, Zarbin MA, Langer P, Guo S, et al. Twelve-year review of pediatric traumatic open globe injuries in an urban U.S. population. J Pediatr Ophthalmol Strabismus. 2012;49:73–9. https://doi.org/10.3928/01913913-20110712-02.
8. Smith B, Regan WF. Blow-out fracture of the orbit; mechanism and correction of internal orbital fracture. Am J Ophthalmol. 1957;44:733–9. https://doi.org/10.1016/0002-9394(76)90774-1.
9. Fujino T, Makino K. Entrapment mechanism and ocular injury in orbital blowout fracture. Plast Reconstr Surg. 1980;65:571–6. https://doi.org/10.1097/00006534-198005000-00004.
10. Skorek A, Kłosowski P, Plichta Ł, Raczyńska D, Zmuda Trzebiatowski M, Lemski P. Posttraumatic orbital emphysema: A Numerical Model. J Ophthalmol. 2014;2014:e231436. https://doi.org/10.1155/2014/231436.
11. Ahmad F, Kirkpatrick WNA, Lyne J, Urdang M, Garey LJ, Waterhouse N. Strain gauge biomechanical evaluation of forces in orbital floor fractures. Br J Plast Surg. 2003;56:3–9. https://doi.org/10.1016/s0007-1226(02)00467-8.
12. Rossi T, Boccassini B, Esposito L, Iossa M, Ruggiero A, Tamburrelli C, et al. The pathogenesis of retinal damage in blunt eye trauma: Finite Element Modeling. Invest Ophthalmol Vis Sci 2011;52:3994–4002. https://doi.org/10.1167/iovs.10-6477.
13. Stitzel JD, Duma SM, Cormier JM, Herring IP. A nonlinear finite element model of the eye with experimental validation for the prediction of globe rupture. Stapp Car Crash J 2002;46:81–102.
14. Cui Y-H, Huang J-F, Cheng S-Y, Wei W, Shang L, Li N, et al. Study on establishment and mechanics application of finite element model of bovine eye. BMC Ophthalmol 2015;15:101. https://doi.org/10.1186/s12886-015-0073-4.
15. Gray W, Sponsel WE, Scribbick FW, Stern AR, Weiss CE, Groth SL, et al. Numerical modeling of paintball impact ocular trauma: identification of progressive injury mechanisms. Invest Ophthalmol Vis Sci 2011;52:7506–13. https://doi.org/10.1167/iovs.11-7942.
16. Kłosowski P, Skorek A, Koberda M. Extended numerical analysis of an eyeball injury under direct impact. Exteneded Numer. Anal. Eyeball Inj. Impact, Cracow, Poland: 2019.
17. Żerdzicki K, Lemski P, Kłosowski P, Skorek A, Zmuda Trzebiatowski MA. Identification of mechanical properties of human orbital wall bones. Columbia University, New York, USA: 2019.
18. Zmuda Trzebiatowski MA, Skorek A. Sophistication assessment of existing FEM models of orbital blowout trauma: Is models valuation justified? J Stomatol Oral Maxillofac Surg. 2020;121:611–3. https://doi.org/10.1016/j.jormas.2020.05.012.
19. Nogueira P, Zankl M, Schlattl H, Vaz P. Dose conversion coefficients for monoenergetic electrons incident on a realistic human eye model with different lens cell populations. Phys Med Biol. 2011;56:6919–34. https://doi.org/10.1088/0031-9155/56/21/010.
20. Uchio E, Ohno S, Kudoh J, Aoki K, Kisielewicz LT. Simulation model of an eyeball based on finite element analysis on a supercomputer. Br J Ophthalmol. 1999;83:1106–11.
21. Nagasao T, Miyamoto J, Nagasao M, Ogata H, Kaneko T, Tamaki T, et al. The effect of striking angle on the buckling mechanism in blowout fracture. Plast Reconstr Surg. 2006;117:2373–80; discussion 2381. https://doi.org/10.1097/01.prs.0000218792.70483.1f.
22. Schaller A, Huempfner-Hierl H, Hemprich A, Hierl T. Biomechanical mechanisms of orbital wall fractures - a transient finite element analysis. J Craniomaxillofac Surg. 2013;41:710–7. https://doi.org/10.1016/j.jcms.2012.02.008.
23. Al-Sukhun J, Lindqvist C, Kontio R. Modelling of orbital deformation using finite-element analysis. J R Soc Interface. 2006;3:255–62. https://doi.org/10.1098/rsif.2005.0084.
24. Al-Sukhun J, Penttilä H, Ashammakhi N. Orbital stress analysis: part III: biomechanics of orbital blowout fracture repair using bioresorbable poly-L/DL-lactide (P[L/DL]

LA 70:30) implant. J Craniofac Surg. 2011;22:1299–303. https://doi.org/10.1097/SCS.0b013e31821c6ae9.

25. Al-Sukhun J, Penttilä H, Ashammakhi N. Orbital stress analysis, part V: systematic approach to validate a finite element model of a human orbit. J Craniofac Surg. 2012;23:669–74. https://doi.org/10.1097/SCS.0b013e31824db8a0.
26. Nagasao T, Miyamoto J, Shimizu Y, Jiang H, Nakajima T. What happens between pure hydraulic and buckling mechanisms of blowout fractures? J Craniomaxillofac Surg. 2010;38:306–13. https://doi.org/10.1016/j.jcms.2009.09.001.
27. Nagasao T, Miyamoto J, Tamaki T, Kanazaki S, Ogawa K. Inferior meatal antrostomy impairs dynamic stability of the orbital walls. Auris Nasus Larynx. 2009;36:431–7. https://doi.org/10.1016/j.anl.2008.09.004.
28. Dai P, Han H, Zhao Y, Fan M. Finite element analysis of the mechanical characteristics of glaucoma. J Mech Med Biol. 2016;16:1650060. https://doi.org/10.1142/S0219519416500603.